NEOPLASIA
www.neoplasia.com

Volume 30 Number xxx Month 2022 pp. 100811



# Longitudinal genomic alternations and clonal dynamics analysis of primary malignant melanoma of the esophagus ☆

Jingjing Li[a,1,*]; Wenyan Guan[b,1]; Wei Ren[c]; Ziyao Liu[a]; Hongyan Wu[b]; Yiqiang Chen[a]; Siyuan Liu[a]; Xiangming Quan[d]; Zuoquan Yang[d]; Chong Jiang[e]; Jian He[e]; Xiao Xiao[d,*]; Qing Ye[a,f,g,*]

[a] The Precision Medicine Centre of Nanjing Drum Tower Hospital, Nanjing University Medical School, Nanjing 210008, Jiangsu, China
[b] The Pathology Department of Nanjing Drum Tower Hospital, Nanjing University Medical School, Nanjing 210008, Jiangsu, China
[c] The Comprehensive Cancer Centre of Drum Tower Hospital, Medical School of Nanjing University & Clinical Cancer Institute of Nanjing University, Nanjing 210008, China
[d] Geneplus-Shenzhen, Shenzhen 518118, China
[e] The Nuclear Medicine Department of Nanjing Drum Tower Hospital, Nanjing University Medical School, Nanjing 210008, Jiangsu, China
[f] Department of Pathology, the First Affiliated Hospital of USTC, Division of Life Sciences and Medicine, University of Science and Technology of China, Hefei, Anhui, 230036, China
[g] Intelligent Pathology Institute, Division of Life Sciences and Medicine, University of Science and Technology of China, Hefei, Anhui, 230036, China

## Abstract

Primary malignant melanoma of the esophagus (PMME) is a rare gastrointestinal melanoma with a high rate of recurrence and metastasis. The standard of care for PMME has not been established yet due to a lack of understanding of its clinical and molecular pathogenesis. Thus, we performed genomic profiling on a recurrent PMME case to seek novel opportunities for the management of this rare disease. Between 2013 and 2016, 6 tissue samples including 3 from the primary tumors, 2 from the relapsed tumors, and 1 from a normal control were collected from a patient diagnosed with PMME and were subjected to whole-exome sequencing to track the dynamic genetic changes. Additionally, we also analyzed a cohort of 398 samples obtained from the TCGA skin cutaneous melanoma (TCGA-SKCM) dataset to assess the frequency and determine the clinical implications of genomic events found in the presented study. *ARHGAP35* (p.L1022M) was the only mutation shared across temporal PMME lesions. The PMME samples showed higher levels of genetic instability and intra-tumor heterogeneity. They also shared several concordant copy number variations (CNV). All lesions were concordant with the evolution trajectory, and shrinkage of the founding clone caused the subclonal population to become dominant in PT1c, which was likely the reason behind metastatic seeding. *ARHGAP35* mutations were found in 6% of the TCGA-SKCM cohort samples. The presence of the mutations was associated with poor progression-free survival (PFS) by both univariate and multivariate Cox regression analyses. Our study showed that the primary tumor clone disseminates earlier in PMME. This highlights the need to understand the mechanism involved in the early PMME recurrence to optimize treatment.

*Neoplasia (2022) 30, 100811*

**Keywords:** Primary malignant melanoma of the esophagus, Early dissemination, ARHGAP35, Dynamic evolution

## Background

Primary malignant melanoma of the esophagus (PMME) is a rare gastrointestinal (GI) melanoma, accounting for 0.1 to 0.2% of all esophageal

*Abbreviations:* PMME, Primary malignant melanoma of the esophagus; GI, Gastrointestinal; FFPE, Formalin-fixed paraffin-embedded; ESD, Endoscopic submucosal dissection; DC-CIK, Dendritic cell-activated cytokine-induced killer cell; DC-CTL, Dendritic cells-cytotoxic T lymphocytes; WES, Whole-exome sequencing; SNVs, Somatic single nucleotide variants; TMB, Tumor mutation burden; SCNVs, Somatic copy number variations; GII, Genome instability index; SBS, Single base substitutions; IHC, Immunohistochemistry; PFS, Progression-free survival; OS, Overall survival; DEGs, differentially expressed genes.

* Corresponding authors.
E-mail addresses: jijilee_82@163.com (J. Li), xiaoxiao@geneplus.org.cn (X. Xiao), qingye1998@ustc.edu.cn (Q. Ye).

☆ The authors declare no potential conflicts of interest.

[1] These authors contribute equally to this paper.

Received 21 February 2022; accepted 16 May 2022



https://doi.org/10.1016/j.neo.2022.100811

cancer and less than 0.05% of all melanoma subtypes. PMME is typically detected at a more advanced stage and tends to display high rates of recurrence and metastasis. About 18.4% of PMME patients present with metastatic disease at the time of diagnosis and 89.7% develop recurrence or metastasis within a few months from diagnosis [1]. As a result, PMME tends to have a poor 5-year overall survival (OS) ranging between 4% to 37.5% [1–4].

In our prior study, PMME tumors displayed a high intra-tumor heterogeneity, and normal mucosa samples carried genetic alternations derived from the primary tumor clone, which suggests the possibility of dissemination during the very early stages of tumorigenesis [5]. Only 483 PMME cases have been reported so far up to 2021 [1,3,5,6]. As a result due to its rarity, the clinical and molecular pathogenesis of PMME is still not understood, and hence the treatment is still not optimized. Thus, there is an urgent clinical need to understand the molecular mechanisms involved in the relapse of PMME.

Therefore in this study, we aimed to further investigate the genomic alternations and clonal dynamics involved in PMME relapse through longitudinal genomic profiling of a patient that developed PMME relapse twice within four years from diagnosis. In addition, we also explored how the genomic profiles evolved in the relapse of PMME under treatment pressure, as well as analyzed of a cohort of 398 samples obtained from the TCGA-SKCM dataset to assess the frequency and determine the clinical implications of genomic events found in the presented study.

## Methods

### *Patient characteristics*

A 68-year-old Chinese female, with a 4-month history of dysphagia and retrosternal burning pain, was admitted to the Thorax Surgical Department of Nanjing Drum Hospital in February 2013. Physical examination and CT scan showed no evidence of skin melanoma lesions. The patient underwent a partial esophagectomy without any treatment before surgery. The resected specimen was a multifocal (three lesions termed as WMY-PT1a, WMY-PT1b, and WMY-PT1c), elevated pigmented tumor measuring 0.4cm × 1.8cm. Histological analysis confirmed mucosal and sub-mucosal melanoma sparing the muscular tunica, without lymph node involvement (0/8 positive) or peripheral nerves and vessels invasion. Immunohistochemical staining demonstrated positive expression of human melanoma black 45 (HMB45), Melan A, and S100. The patient received one week chemotherapy with fotemustine and oxaliplatin as adjuvant therapy and stopped chemotherapy for intolerance. Instead, the patient was treated with five treatments of dendritic cell (DC)–cytokine–induced killer (CIK) (DC-CIK) immunotherapy combined with Recombinant human interleukin 2 and Recombinant human granulocyte macrophage stimulating factor within one month. In September 2014, esophagogastroscopy revealed two elevated tumors at 24 cm from the incisors (WMY-R1). The lesions were removed via endoscopic submucosal dissection (ESD) and postoperative pathological examination confirmed the presence of a PMME diagnosis. After surgery, the patient received additional immunotherapy using temozolomide combined with dendritic cell-cytotoxic T lymphocytes (DC-CTLs) for two weeks. A second relapse (WMY-R2) was identified in June 2016 following an endoscopy examination. The patient then underwent ESD treatment and postoperative pathological examination which again confirmed a PMME diagnosis. In August 2016, an abdominal computed tomography (CT) revealed a mass in the right lobe of the liver. Positron Emission Tomography-Computed Tomography (FDG PET/CT) showed hypermetabolic lesions in the right liver lobe with a maximum standardized uptake value of 7.5 (Fig.S1). The patient was diagnosed with liver metastasis and died in November 2016.

This study was approved by the Internal Review Board of Nanjing Drum Tower Hospital and was conducted in accordance with the Declaration of Helsinki (Revised in 2013).

### *Extraction of tissue samples*

Six formalin-fixed paraffin-embedded (FFPE) tissue samples including three primary PMME tumor samples, one normal esophageal mucosa sample, and two relapsed tumor samples were collected from the same patient (Fig. 1). Genomic deoxyribose nucleic acid (DNA) was isolated using the TIANamp Genomic DNA kit (Tiangen Biotech, Beijing, China) according to the manufacturer's instructions.

### *Whole-exome sequencing*

The DNA of the PMME tumor and normal samples was fragmented with an ultrasonicator UCD-200 (Diagenode, Seraing, Belgium), and subsequently purified and selected according to size with Ampure Beads (Beckman, MA, USA) following end repairing, an "A" base addition and adaptor ligation. The purity and concentration of the DNA were determined using a Nanodrop 2000 spectrophotometer and a Qubit 2.0 Fluorometer with Quanti-IT dsDNA HS Assay Kit (Thermo Fisher Scientific, MA, USA). Samples were prepared using the TruSeq Capture kit (Illumina, San Diego, CA, USA) for DNA libraries preparation. Whole exome paired-end sequencing was performed on Illumina HiSeq X10 (Illumina, San Diego, CA, USA) at Novegene (Novegene, Beijing, China). After filtering out the low-quality reads and reads containing adaptor sequence, the raw reads were mapped to the reference human genome (hg19) by using the BWA aligner (version 0.7.10). For quality control purposes the BAM files with target sequences at an average depth of 180 × for the tumors and 150 × for normal samples were kept.

### *Annotations of the somatic single nucleotide variants (SNVs) and small insertions and deletions (indels) variants*

The normal mucosal samples served as germline control. SNVs and indels were identified by using MuTect2 packed in GATK (version 4.1.2.0). Reliable variants were acquired for the following three types of variants; (i) variants with allele frequency above or equal to 0.01; (ii) variants with mutations as indicated in public databases (1000 Genomes, gnomAD, and ExAC) with allele frequency below or equal to 0.001; (iii) variants located in the coding region of the genome. The latter variants were defined as functional variants and kept for all analysis except for signature decomposition.

Putative driver genes were curated by merging the COMSIC Cancer Gene Census (https://cancer.sanger.ac.uk/census, v90) and those reported by Bailey *et al.* [7] and Vogelstein *et al.* [8]. Sorting Intolerant from Tolerant (SIFT) and Polymorphism Phenotyping-2 (Polyphen2) were used to identify the putative driver mutations. Missense mutations identified as deleterious by either of these two algorithms were classified as putative driver mutations. The tumor mutation burden (TMB) was defined as the number of somatic coding non-synonymous variants per megabase of genome examined (33 Mb). Furthermore, the Cancer Genome Atlas (TCGA) database was searched to acquire the MAF files and the corresponding clinical data. A total of 398 skin cutaneous melanoma (SKCM) samples were downloaded from the cBioportal (http://www.cbioportal.org/, October 2021) and were subjected to the uniform in-house filter pipeline to improve the unity of the data from different origins.

### *Somatic copy number variation (sCNV) calling*

ABSOLUTE was used to estimate genome ploidy to determine the allele-specific DNA copy number. Based on the major (a2) and minor (a1) allele

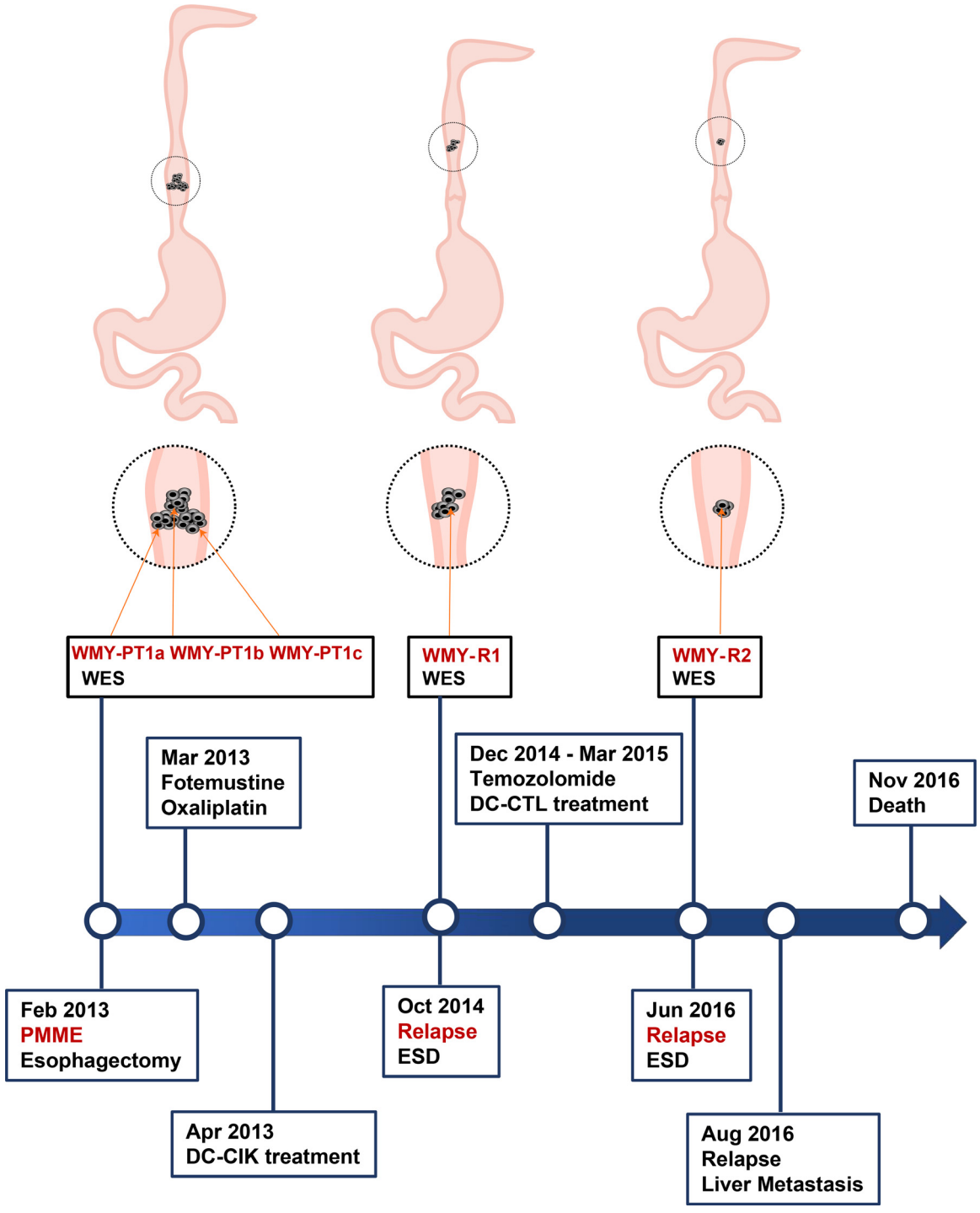


**Figure 1.** Treatment pathway diagram and sites of histological specimens collected for whole exome sequencing. Abbreviations: PMME, primary malignant melanoma of the esophagus; ESD, endoscopic submucosal dissection; DC-CIK, dendritic cell-activated cytokine-induced killer cell; DC-CTL, dendritic cells-cytotoxic T lymphocytes; WES, whole-exome sequencing.

copy number, the sCNVs were classified as duplicated (a1+a2 > 2 and a1 > 0), haploid loss of heterozygosity (LOH) (a2 = 1, a1 = 0), copy number neutral LOH (a2 = 2, a1 = 0), duplication LOH (a2 > 2, a1 = 0) and homogeneous deletion (a1 = a2 = 0). To better reflect the CNV amplification and deletion, the log2 ratio was calculated and used to gauge the CNV frequency of each cohort based on a threshold of 0.15, and subsequently used to estimate the genome instability index (GII), which was defined as the proportion of the length of the genome with a segmented copy number amplification ($GII_{Amp}$) or deletion ($GII_{Del}$).

### *Dynamic clone evolution inference*

The cancer cell fractions (CCF) of each mutation were estimated by ABSOLUTE. PyClone-VI [9] and clonevol [10] were used to infer seeding

patterns associated with the primary tumor and relapsed tumors. The PyClone-VI consensus cluster files were used to enumerate the evolutionary relationships, and the evolutionary trajectory between clones was estimated by clonevol and visualized by Fishplot [11].

### *Reconstruction of the phylogenetic tree*

PYLIP [12] was applied to reconstruct the phylogeny of recurrent PMME using all non-synonymous mutations identified by WES. The maximum parsimony algorithm was adopted to build the optimal tree structure. In this case, mutations shared by all five samples and less than five samples were defined as trunk and branch events respectively, while mutations harbored by only one sample were defined as private events.

### *Analysis of mutational signature and pathway enrichment*

The Yet Another Package for Signature Analysis (YAPSA), version 3.12 was employed to analyze the mutational signature of single base substitutions (SBS) according to the COSMIC database [13]. To better display the dynamics of mutational signature based on the phylogenetic tree, the signature composition of each branch were analyzed by the mutations of the tree, which were annotated as specific signatures by using the YAPSA package [14].

The pathway enrichment of the mutated genes from different phylogenetic clades were based on the Kyoto Encyclopedia of Genes and Genomes (KEGG) database and were analyzed using the R package clusterProfiler. The g:Profiler(https://biit.cs.ut.ee/gprofiler/gost) was used to compare the altered pathways enriched by differentially expressed genes (DEGs) between the *ARHGAP35*-wild type and *ARHGAP35*-mutant groups derived from the TCGA SKCM cohort. These DEGs were identified using the limma package with a false discovery rate (FDR) adjusted *p*-value of less than 0.05 and an absolute log2 fold change value of more than 1.

### *Immune infiltration level and immune therapy response prediction*

The level of tumor-infiltrating immune cells of the SKCM samples obtained from TCGA was analyzed by TIMER2.0. TIMER is an interactive web server for online analysis and visualization of immune cell infiltration (timer.comp-genomics.org) [15]. According to the developer's instructions, we performed the comparison between *ARHGAP35*-mutant and *ARHGAP35*-wildtype SKCM samples by using the "Mutation" module belonging to the "Immune Association" tab and used the CIBERSORT results for further interpretation.

### *Immunochemistry (IHC)*

The transforming RhoA/B/C protein expressions of the PMME tumor were assessed by IHC staining. The specimens were fixed in formalin and embedded in paraffin. Tissue sections of a thickness of 3μm were deparaffinized in xylene and rehydrated. Heat-mediated antigen retrieval was performed with ethylenediaminetetraacetic acid (EDTA) buffer solution with a pH of 9.0 before commencing with IHC staining protocol. Then the sections were incubated with an anti-RhoA/B/C antibody (1:20000, Boster Biological Technology Co. Ltd., China) overnight at 4°C, and subsequently washed three times with phosphate-buffered saline (PBS). Thereafter, the sections were incubated with a Goat Anti-Rabbit IgG H&L (HRP) secondary antibody (1:500, Boster Biological Technology Co.Ltd., China) for 30 min at 37°C, and again washed three times with PBS. The peroxidase activity was visualized by using a diamino-benzidine tetrahydroxy chloride solution. The sections were counterstained with hematoxylin. Positive control section samples for RhoA/B/C were obtained from tonsillar tissue, while the negative control section samples were obtained from normal liver tissue. The immunoreactivity of RhoA/B/C was assessed independently by two pathologists who were blinded to the clinical background of the patients, and would ask for a third party to make a judgement when there was disagreement. Specimens with clear evidence of membrane and cytoplasm staining were considered immunopositive.

### *Statistical analysis*

The two-sided Mann-Whitney *U* test was employed for the comparisons between two groups of continuous data using Graphpad Prism (version 8.0). Survival analysis was performed using the survival package in R (version 4.0.2). The hazard ratio (HR) was calculated by the univariate Cox proportional hazards model. The Kaplan-Meier methodology was applied for the comparison of overall survival (OS) and progression-free survival (PFS) between groups and the *p*-value was calculated by the Log-rank test. For the SKCM cohort, the OS and PFS were obtained from the clinical data available on the TCGA database. All statistical tests were two-sided and a *p*-value below 0.05 was considered statistically significant.

## Results

### *The repertoire of somatic mutations and copy number alterations among samples*

Whole-exome sequences were covered by a median coverage of 238 × (range from 184 to 385) for the five PMME samples and 167 × for the normal control sample, with an average of 80% coverage of the targeted regions represented by at least 100 reads. The main composition of variant classification of mutations among these samples was missense mutations, and there were also appreciable numbers of in-frame deletions and insertions (Fig. 2A). Overall, the five PMME samples displayed low TMB, with a median of 2.7 mutations (range,1.8-3.3), and showed a highly concordant SBS pattern, consisting of a high proportion of cytosine (C) and a smaller portion of thymine (T) and adenine (A) (Fig. 2B). Mutational signature analysis revealed that the SBS1 and 5 (clock-like) were dominant among all tumors, and SBS19 (unknown), SBS24 (aflatoxin exposure), and SBS39 (unknown) were also present across primary and recurrent tumors (Fig. 2C). Interestingly, SBS22 (aristolochic acid exposure) disappeared in the WMY-R1 site but occurred again in the WMY-R2 site.

The genomic instability between the primary PMME and recurrences was compared. sCNVs analysis revealed a common copy number gain on chromosomes 6p, 8q, 19q, and 20p, as well as loss of chromosomes 6q and 10p across both the primary and relapsed PMME sites (Fig. 2D and Fig. S2). Additionally, the relapsed PMMEs showed higher microsatellite instability than that of three primary samples and tended to have a higher GII score (Fig. 2D and E), suggesting that the recurrent genome was more unstable during tumor progression.

### *Potential driver genesof PMME*

We then analyzed the somatic alterations in known cancer driver genes that were predicted to have functionally deleterious effects by using SIFT and POLYPHEN, and identified several potential driver genes including *ARHGAP35, SF3B1, TRRAP, NF1, FOXO1, KMT2C, MAP3K1, CREBBP*, and *NRAS*, as well as copy number amplifications of genes including *ARHGAP35, FAM135B, CDKN1A*, and loss of *EPHA7, CDKN2A, PTEN* (Fig. 2E). Collectively, the genetic features of the PMME in our case analysis were consistent with previous melanoma sequencing studies [16]. After comparing the genomic features of the primary tumors and recurrences, mutations affecting several melanoma-related genes such as *NRAS* and *MAP3K1* and copy number amplification of *KRAS* were only identified in

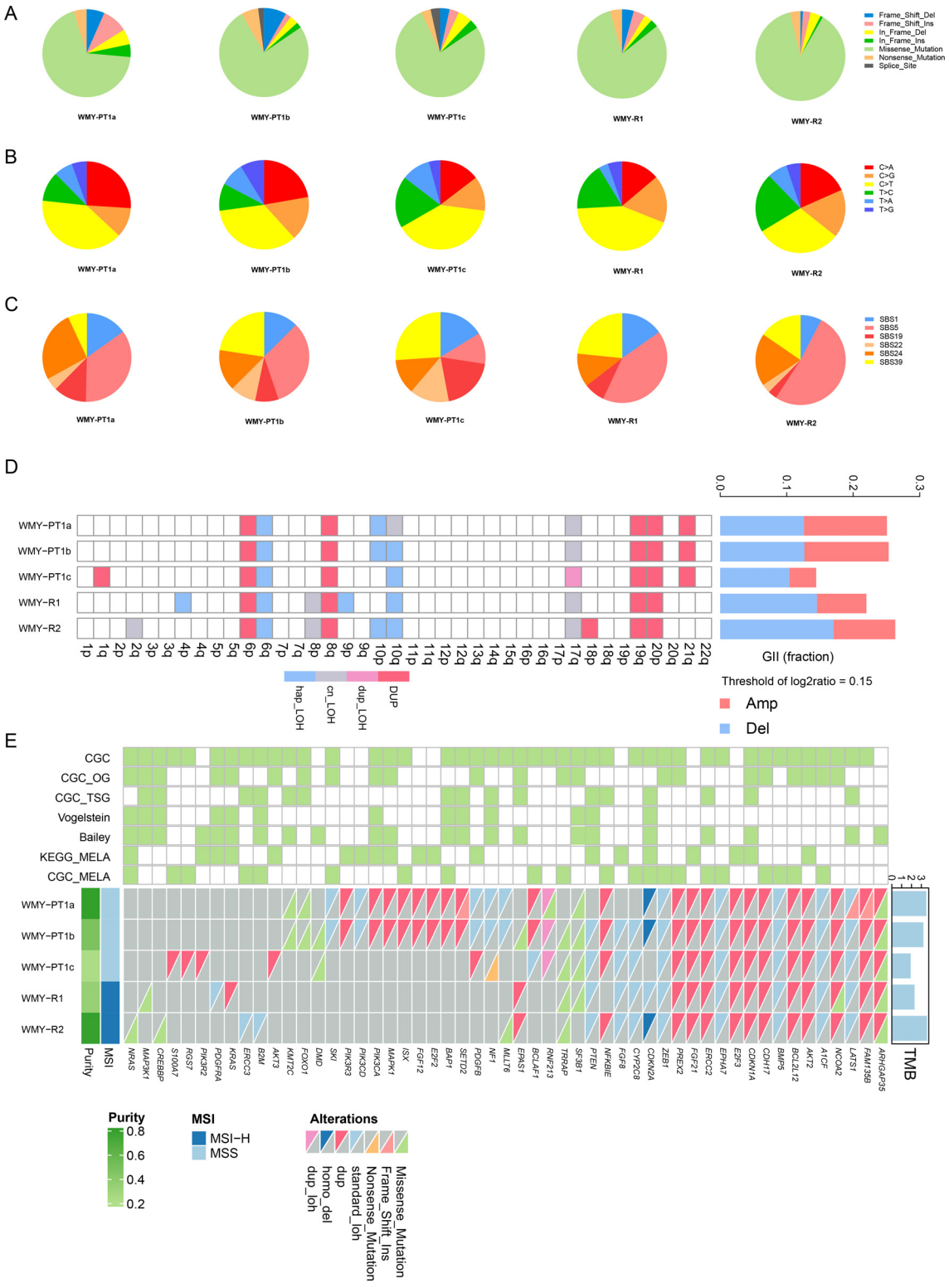


**Figure 2.** Repertoire of somatic mutations and copy number alterations within the acquired samples. (A-C) Pie charts showing the composition of single variant classification (A), base substitution (B), and mutational signature (C) in each sample. (D)Arm-level CNV identified in samples. Amplification (DUP/dup_LOH), copy-neutral LOH, and deletion (only haploid_LOH in this case) are displayed. Genome instability index (GII) divided into amplification and deletion parts was calculated. (E) The landscape of driver mutations (see methods) and CNV of the selected genes (genes with driver mutations and melanoma genes defined by KEGG and Cancer Gene Census). Volgelstein refers to the PMID: 23539594 study and Bailey refers to the PMID: 29625053 study. Abbreviations: CGC, Cancer Gene Census; CGC_OC, oncogene annotated by CGC; CGC_TSG, tumor suppressor gene annotated by CGC; KEGG_MELA, melanoma genes annotated by KEGG; CGC_MELA, melanoma genes annotated by CGC. MSI-H, high microsatellite instability; MSS, microsatellite stable; TMB, tumor mutation burden; LOH, loss of heterozygosity.

the relapsed sites. The *NF1* mutation was only detected in the WMY-PT1c suggesting that tumor clones with *NF1* mutation may be either sensitive to DC-CIK treatment or have a disadvantage in tumor cell competition. Notably, *ARHGAP35* was the only mutated gene shared by all five samples, simultaneously affected by both CNV and SNV, indicating the importance of this gene in the development or maintenance of PMME.

### *The evolutionary trajectoryof PMME*

To better understand the evolutionary origins of recurrent PMME, a phylogenetic tree was constructed based on the high confidence mutations identified in each tumor cell affected region for all primary tumor samples and recurrent samples (Fig. 3A).The topological structure of the tree showed that this PMME complied with the branch evolutionary model and could be divided into two clades: (i) primary clade including WMY-PT1a and WMY-PT1b; (ii) relapsed clade including WMY-R1, WMY-R2, and WMY-PT1c (Fig. 3A).

Although these samples displayed a high degree of inter-sample heterogeneity, a total of 20 gene mutations were found to be shared among all samples (Fig. 3B-C, Table S1). However, the $ARHGAP35^{L1022M}$ gene mutation was identified as the only driver mutation along the trunk. In the primary clade, $FOXO1^{A172D}$and $KMT2C^{P3169S}$ driver mutations were observed in the branch while *EPAS1, LATS1, SETD2,* and *FAM135* mutations were private. No significant branch mutation was observed in the relapsed clade, and the well-defined melanoma genes such as *NF1* and *NRAS* occurred as private mutations in the WMY-PT1c and WMY-R2 samples, respectively. CNV alternations were added to the phylogenetic tree according to the extent of shared somatic CNVs identified in each sample. Amplifications of *ARHGAP35, FAM135, CDH17, CDKN1A, AKT2,* and *FGF21,* as well as loss of *EPHA7, ZEB1, BMP5,* and *LATS1* were ubiquitous and were conserved across all PMME samples (Fig. 2E, Fig. 3A, and Fig S2). The *SF3B1* and *TRRAP* mutants were also identified in intermixed tumor clones by CCF analysis (Fig. S3A-B), suggesting a multiclonal origin. Similarly, the results based on SNVs, common sCNVs, and chromosome alternations were also found to be shared by WMY-PT1c and recurrent samples. Collectively, phylogeny analysis inferred that PMME dissemination occurred during the primary tumor initiation and the invisible metastatic colonization may therefore account for the two recurrences.

We next depicted the mutational signature tree based on analyzing the somatic mutations from each determined phylogenetic class (Fig. 3D). SBS15, 24, and 39 were identified as dominant mutational signatures. After comparing the mutational signature landscape (Fig. 2C), SBS1, 5, and 22 disappeared reflecting the existence of the intermixed tumor clone and high intra-tumor heterogeneity within the PMME. Interestingly, SBS24 (ascribed to aflatoxin exposure) was lost in the early recurrences (WMY-PT1c and WMY-R1) but became active again in the late recurrence site (WMY-R2). The temporal episodic mutational signature suggested that the progenitor tumor clone could be dormant after seeding until an adapted microenvironment was reconstructed.

The altered gene pathways were further investigated in both the primary and relapsed clades. The mutated genes in the relapse clade (annotated in Fig. 3A) tended to be enriched in axon guidance and TGF-beta signaling pathways (Fig. 3E), both of which were reportedly involved in metastasis [17,18], while no significant pathway was identified in the primary clade (Fig. S3C).

### *Temporal clonal dynamics of PMME*

The evolutionary relationships and temporal order of the driver acquisitions during the PMME progression were evaluated by calculating the CCF value of SNVs and indels of the affected canonical driver genes. To further explore the relationship between each tumor site, we compared the CCF between each two of the five samples. The results showed a significant correlation between WMY-PT1a and WMY-PT1b, as well as WMY-R1 and WMY-R2 (Fig. 4A). The clonality of mutations represented by the CCF distribution increased in the recurrent lesions (Fig. 4B), either by using all mutations (left panel of Fig. 4B) or private mutations (right panel of Fig. 4B), suggesting that the recurrent tumors tended to have higher clonality compared to the late-stage primary tumors. The temporal evolution trajectory of clonal dynamics revealed a linear evolution pattern that all lesions were concordant in the evolution trajectory (Fig. 4C). The ancestor clone shrunk during tumor progression and a subclone expansion was observed in WMY-PT1c. Mutations in the *ARHGAP35, SF3B1, TRRAP, MLLT6, FOXO1, NF1, and NRAS genes* (Fig. 4C and Fig.S3) were noted in the dominant subclone, but only the *ARHGAP35* mutation was ubiquitously shared across time. However, no mutations in the cancer-related genes were observed in the founding clone (Fig. 4C). The non-driver genes whose mutations clustered in the founding clone were further analyzed by evaluating the mutation prevalence in the TCGA-SKCM cohort and we found that *RP1, ABCA13,* and *DCDC1* were frequently mutated. However, the role of these genes as driver genes in SKCM had not been reported previously (Fig. S4). Therefore, our results showed that recurrences from the initial tumor were derived by subclonal evolution. In summary, subclonal driver gene mutations were pervasive in this case, indicating the strong positive selection during the tumor progression.

### *The clinical relevance of* ARHGAP35

We specifically focused on the *ARHGAP35* as it represented the only ubiquitously shared driver mutation and consistently maintained a growth advantage from the primary to recurrence stage. In order to explore the clinical value of the *ARHGAP35* mutation in melanoma, we conducted a further analysis based on the TCGA SKCM dataset downloaded from the cBioPortal database. A total of 24 SKCMs (6.03%, 24/398) had the *ARHGAP35* mutations, including 3 nonsense mutations, 24 missense mutations, and 1 inframe deletion (Fig. 5a). These mutations were nearly evenly distributed throughout the coding sequence but lacked a hotspot mutation site (Fig. 5a), which indicates that *ARHGAP35* might play a suppressor role in melanoma. Co-occurrence of *ARHGAP35* mutation and other known melanoma driver genes was observed, such as *NF1, PTPRT,* and *FAT4* (Fig. 5B). The survival analysis in the SKCM cohort revealed that the *ARHGAP35* mutation was associated with poor survival. According to univariate analysis, SKCM patients with the *ARHGAP35* mutation had significantly worse OS ($P = 0.006$) and PFS ($P < 0.001$) when compared with those having the wild-type gene (Fig. 5C). Multivariate Cox regression was further carried out to adjust for the effect of clinical parameters and other genes significantly associated with survival by univariate analysis (Fig. 5D-I). After the adjustment, the *RAC1* ($P = 0.027$) and *ARHGAP35* ($P < 0.001$) remained significant predictors of poor PFS (Fig. 5J), however, no significant predictors for OS were identified (Fig. 5K).

### *Exploring the potential function of the* ARHGAP35*mutation*

In order to get further insight into the potential biological function of the *ARHGAP35* mutation, we investigated the immune activity and the global transcriptomic change between the *ARHGAP35*-mutant and the wild-type patients in the TCGA-SKCM cohort. According to the CIBERSORT analysis, when compared with the *ARHGAP35* wild-type patients, the *ARHGAP35* mutated patients exhibited a significant fraction reduction in the resting myeloid DC cells and a significant fraction increase in the naive CD4+ T-cells and naive B-cells (Fig. S5A-C). Furthermore, the down-regulated genes in the *ARHGAP35* mutated group were significantly enriched in Gene Ontology terms of adaptive immune response and immune system process (Fig. S5D), while no pathway was enriched by the up-regulated genes.

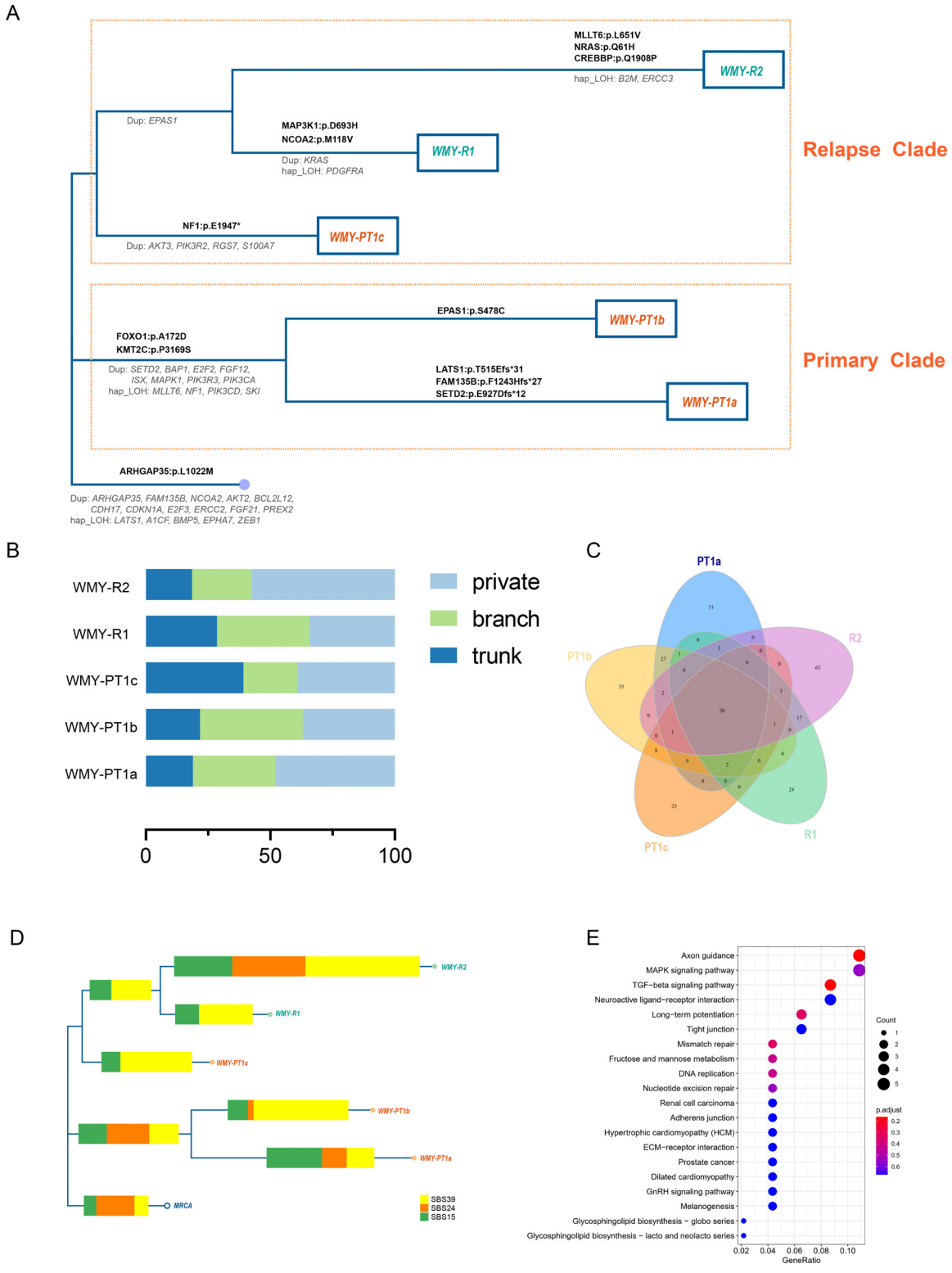


**Figure 3.** Phylogeny inference based on somatic mutations across the five samples. (A) The phylogenetic structure was established according to the presence and absence of somatic mutations. The orange rectangle indicates the evolutionary clade. The gray fonts illustrate the CNV changes, while the black bold fonts show key mutations. (B and C) Stacked bar plot showing the percentage (B) and Venn plot showing the absolute number (C) of shared and private mutations among the five samples. (D) Mutational processes were inferred based on mutations along with different segments of the phylogenetic tree (A). (E) KEGG pathways enriched by the mutated genes within the relapse clade (A). Abbreviations: Dup, duplication; hap_LOH, haploid loss of heterozygosity.

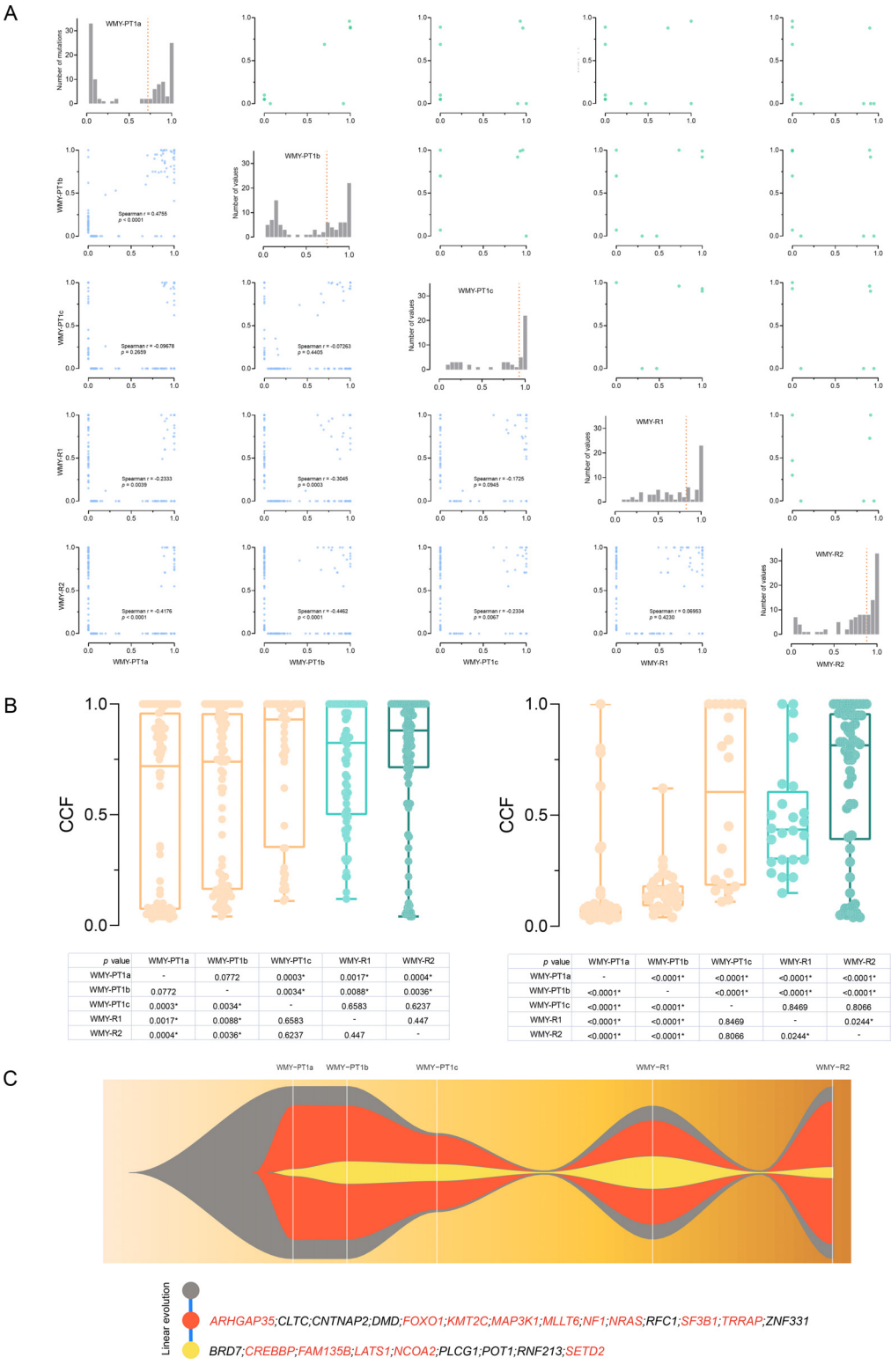


| p value | WMY-PT1a | WMY-PT1b | WMY-PT1c | WMY-R1 | WMY-R2 |
|---|---|---|---|---|---|
| WMY-PT1a | - | 0.0772 | 0.0003* | 0.0017* | 0.0004* |
| WMY-PT1b | 0.0772 | - | 0.0034* | 0.0088* | 0.0036* |
| WMY-PT1c | 0.0003* | 0.0034* | - | 0.6583 | 0.6237 |
| WMY-R1 | 0.0017* | 0.0088* | 0.6583 | - | 0.447 |
| WMY-R2 | 0.0004* | 0.0036* | 0.6237 | 0.447 | - |

| p value | WMY-PT1a | WMY-PT1b | WMY-PT1c | WMY-R1 | WMY-R2 |
|---|---|---|---|---|---|
| WMY-PT1a | - | <0.0001* | <0.0001* | <0.0001* | <0.0001* |
| WMY-PT1b | <0.0001* | - | <0.0001* | <0.0001* | <0.0001* |
| WMY-PT1c | <0.0001* | <0.0001* | - | 0.8469 | 0.8066 |
| WMY-R1 | <0.0001* | <0.0001* | 0.8469 | - | 0.0244* |
| WMY-R2 | <0.0001* | <0.0001* | 0.8066 | 0.0244* | - |

**Figure 4.** Dynamics of the PMME clonal evolution. (A) Scatter plot comparing the cancer cell fraction (CCF) between each two of the five samples. Lower left triangle, all mutations; Diagonal line, distribution of CCF of mutations in each sample; Upper right triangle, driver mutations. (B) Boxplot comparing CCF of all mutations (left panel) and CCF of private mutations (right panel) which represent the late-stage alterations between samples. *p*-values were generated by the Mann-Whitney *U* test. (C) Fishpot depicting a linear evolution pattern (estimated by clonevol) of putative clones (estimated by PyClone-VI). Driver genes in each clone are annotated and those with driver mutations are in red. The founding clone is illustrated in grey and the subclone is illustrated in tangerine, and yellow.

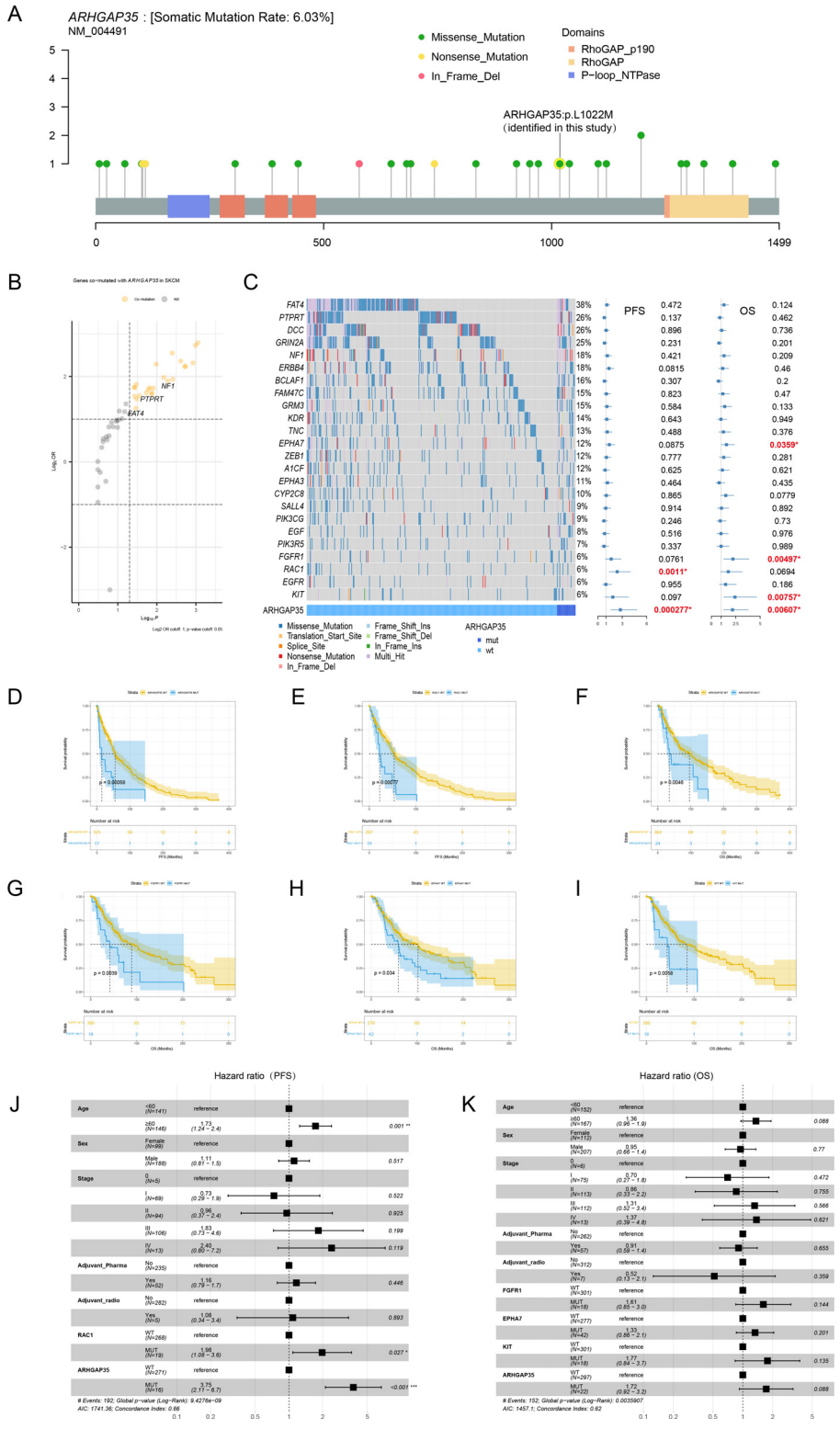


**Figure 5.** *ARHGAP35* mutation was associated with the clinical outcome of skin cutaneous melanoma. These analyses were based on the data of 398 skin cutaneous melanoma (SKCM) samples from TCGA. (A) The comparison of the spectrum of somatic mutations affecting *ARHGAP35* in the TCGA SKCM cohort and the one identified in the patient from our study. (B) Scatter diagram showing melanoma genes co-mutated with *ARHGAP35* (yellow). (C) Mutational landscape (left) of the genes co-mutated with *ARHGAP35*, corresponding with forest-plot (right) indicating the association of these genes with PFS and OS (right, univariate Cox regression model). (D-I) KMplots and log-rank *p*-values of genes whose mutation status significantly affected the PFS or OS. (J-K) Multivariate Cox regression was carried out to adjust for the effect of clinical parameters on PFS (J) and OS (K), respectively.

The protein-protein interaction networks based on STRING showed strong experimental and bioinformatic evidence that ARHGAP35 could interact with RHOA, RAC1, and RASA1 (Fig. S5E). The Rho activity was suppressed by GAPs and p190A. The RhoGAP encoded by the *ARHGAP35* gene was generally regarded as the main RhoGAP for RhoA in cells, so we speculated that the protein expression of Rho GTPases might have changed in this PMME patient. The IHC results showed that Rho GTPases were expressed positively in the cytoplasm and membrane of tumor samples, and negatively in the normal sample (Fig. S5F).

## Discussion

In this manuscript, we describe a rare case of a female patient diagnosed with PMME who underwent three surgical treatments to remove the primary tumor and subsequently two recurrences. According to the pathological examination, the resected tumors had negative surgical margins and there was no evidence of metastasis at the time of the surgical resection. Given that 5cm of the esophagus had been removed at the first surgery, our analysis on driver gene heterogeneity and clonality revealed that subclones in recurrences stemmed from the initial tumor, suggesting that early dissemination extended beyond the surgical resection. The hypothesis that the recurrent subclone was derived from one of the primary tumors was supported by the results of the phylogenetic tree based on SNVs, CNVs, and mutational signatures. It should be noted that no potential driver genes or pathways were identified in the founding clone, suggesting that the founding clone had the ability of cell migration but still needed further gene regulation by mechanism such as epigenetic modification to invoke cell proliferation. It seems that the subclones in the later relapsed sites were in a dormant state until a change in the environment triggered their rapid proliferative potential.

*ARHGAP35*, a less well-known driver gene, was the only significant trunk mutated gene identified among these samples. *ARHGAP35* encodes p190RhoGAP-A which has been considered to be a tumor suppressor gene and involved in cell-cell junctions and cell migration by regulating RhoA activity [19]. The other PMME cases we reported before also had genetic alternations within the guanine nucleotide exchange factors (GEFs) and GTPase-activating proteins (GAPs) in the metastatic clade, which are two subsets of regulators controlling the guanosine diphosphate (GDP)/guanosine triphosphate (GTP) cycle of Rho GTPase [20]. Based on our analysis of the TCGA SKCM cohort, the presence of *ARHGAP35* mutations was an independent predictor of poor prognosis and survival in melanoma. We also found that the *ARHGAP35* deficient melanomas showed lower fractions of myeloid DC, naïve CD4+ T cell, and naïve B cell, and had a lower adaptive immune response. Therefore based on the above findings the *ARHGAP35* was identified as a new potential driver gene accounting for metastasis.

Most acquired driver mutations related to tumor growth were private mutations, such as driver mutations in genes *SETD2* and *LATS1* in WMY-PT1a, *EPAS1* in WMY-PT1b, *NF1* in WMY-PT1c, *MAP3K1* in WMY-R1, and *NRAS* in WMY-R2. There is a theory suggesting that early disseminated tumor cells (DTCs) create a niche environment for tumor recurrences such as immunosuppression or metastasis, and cells are often slowly cycling until a change in environment generates a rapid proliferative potential [21]. During this time, expansion of residual disseminated cancer is paused and DTCs survive to fuel relapse and evade anti-proliferative treatment [22–24]. Our findings also support the above theory by phylogenetic evidence based on mutational signature analysis. We found an episodic mutational signature SBS24 disappeared in WMY-PT1c but reproduced in late recurrence WMY-R2 (Fig. 3D), indicating that subclones that originated from the initial clone might have survived the therapy by dormancy.

Gene clustering analysis based on the driver mutations showed that pathways of axon guidance, MAPK, and TGF-beta signaling were abnormal in the relapse clade, however, no significant abnormal pathway was identified in the primary clade. MAPK cascade activation is the center of a variety of signaling pathways and plays a key role in cell proliferation-related signaling pathways. Late acquired private mutations such as those in *MAP3K1, NRAS* and *NF1* were critical nodes in the MAPK pathway, which may have enabled the proliferation ability of DTCs. Axon guidance and TGF-beta signaling are both related to tumor metastasis, suggesting that systemic inhibition of TGF-beta signaling could awake dormant DTCs fueling multi-organ metastasis [25].

It still remains unclear how dormant DTCs evade recognition by the immune system. By utilizing RNA-seq and WES data from TCGA SKCM cohort, we found that *ARHGAP35* mutation was associated with decreased adaptive immune response, as shown by the down-regulated genes enriched within the immune system process and adaptive immune response in the *ARHGAP35* mutant group (Fig.S5A-D). An interesting finding was that the myeloid DCs decreased significantly as well in the mutated group, and the DCs acted as the primary antigen-presenting cells in the tumor and played a critical role in anti-tumor immunity [26,27]. It has been proposed that an initial tumor clone may create the pre-metastatic niche to develop a favorable immune microenvironment and progressively adapt to immune pressure during dissemination [28,29]. Thus, we hypothesize that inactivation of the *ARHGAP35* gene may mediate the mechanisms to modulate DCs and the dysfunctional DCs, facilitating local and metastatic progression. However, further research is warranted to confirm this hypothesis.

## Conclusion

In summary, we demonstrate that the primary PMME tumor can seed from the esophagus, leading to recurrence. This highlights the need to understand the mechanism involved in the early PMME recurrence to optimize treatment. Our data shows that *ARHGAP35* has an important role in promoting metastasis and immune suppression. The involvement of this mutation in tumor recurrence was rarely studied in melanoma. Further research should focus on understanding the role of this mutation in early metastasis, particularly the formation of invisible metastatic colonization, which is essential for the future development of precision therapy and prevention of metastasis in PMME and other melanoma subtypes.

## Data availability

The sequence reported in this paper has been deposited in the CNGBdb (China National GeneBank database, https://www.cngb.org) with accession number CNP0001947. The information of sequencing quality control is showed in Table S2.

## Novelty & impact statements

Primary malignant melanoma of the esophagus (PMME) is a rare aggressive melanoma with a high potential for metastasis and recurrence. However, the standard-of-care treatments for PMME have not been established yet due to a lack of understanding about the clinical and molecular pathogenesis of this rare disease. Our study demonstrated the importance of longitudinal genomic profiling to understand the dynamic nature of recurrence and provided novel evidence to early tumor cell dissemination theory. We also identified a less well known gene *ARHGAP35* as a potential metastasis driver gene in melanoma.

## Funding information

This study was supported by National Natural Science Foundation of China (81902508).

## CRediT authorship contribution statement

**Jingjing Li:** Conceptualization, Methodology, Investigation, Data curation, Writing – original draft, Project administration, Funding acquisition. **Wenyan Guan:** Methodology, Validation, Formal analysis, Investigation, Resources. **Wei Ren:** Writing – review & editing. **Ziyao Liu:** Validation, Formal analysis. **Hongyan Wu:** Methodology, Validation. **Yiqiang Chen:** Formal analysis. **Siyuan Liu:** Formal analysis. **Xiangming Quan:** Software. **Zuoquan Yang:** Software, Visualization. **Chong Jiang:** Visualization. **Jian He:** Writing – review & editing. **Xiao Xiao:** Data curation, Writing – original draft, Project administration. **Qing Ye:** Conceptualization, Resources, Writing – review & editing, Supervision, Project administration.

## Acknowledgments

We thank the patient and her family for participating in this study.

## References

[1] Wang X, Kong Y, Chi Z, Sheng X, Cui C, Mao L, Lian B, Tang B, Yan X, Si L, et al. Primary malignant melanoma of the esophagus: a retrospective analysis of clinical features, management, and survival of 76 patients. *Thorac Cancer* 2019;**10**:950–6.

[2] Iwasaki K, Ota Y, Yamada E, Takahashi K, Watanabe T, Makuuchi Y, Suda T, Osaka Y, Seshimo A, Katsumata K, et al. Primary malignant melanoma of the esophagus with multiple lymph node metastases: a case report and literature review. *Medicine (Baltimore)* 2020;**99**:e18573.

[3] Lasota J, Kowalik A, Felisiak-Golabek A, Zieba S, Waloszczyk P, Masiuk M, Wejman J, Szumilo J, Miettinen M. Primary malignant melanoma of esophagus: clinicopathologic characterization of 20 cases including molecular genetic profiling of 15 tumors. *Mod Pathol* 2019;**32**:957–66.

[4] Chen H, Fu Q, Sun K. Characteristics and prognosis of primary malignant melanoma of the esophagus. *Medicine (Baltimore)* 2020;**99**:e20957.

[5] Li J, Yan S, Liu Z, Zhou Y, Pan Y, Yuan W, Liu M, Tan Q, Tian G, Dong B, et al. Multiregional sequencing reveals genomic alterations and clonal dynamics in primary malignant melanoma of the esophagus. *Cancer Res* 2018; **78**:338–47.

[6] Tsuyama S, Kohsaka S, Hayashi T, Suehara Y, Hashimoto T, Kajiyama Y, Tsurumaru M, Ueno T, Mano H, Yao T, et al. Comprehensive clinicopathological and molecular analysis of primary malignant melanoma of the oesophagus. *Histopathology* 2021;**78**:240–51.

[7] Bailey MH, Tokheim C, Porta-Pardo E, Sengupta S, Bertrand D, Weerasinghe A, Colaprico A, Wendl MC, Kim J, Reardon B, et al. Comprehensive characterization of cancer driver genes and mutations. *Cell* 2018;**173**:371–85 e318.

[8] Vogelstein B, Papadopoulos N, Velculescu VE, Zhou S, Diaz LA Jr, Kinzler KW. Cancer genome landscapes. *Science* 2013;**339**:1546–58.

[9] Gillis S, Roth A. PyClone-VI: scalable inference of clonal population structures using whole genome data. *BMC Bioinf* 2020;**21**:571.

[10] Dang HX, White BS, Foltz SM, Miller CA, Luo J, Fields RC, Maher CA. ClonEvol: clonal ordering and visualization in cancer sequencing. *Ann Oncol* 2017;**28**:3076–82.

[11] Miller CA, McMichael J, Dang HX, Maher CA, Ding L, Ley TJ, Mardis ER, Wilson RK. Visualizing tumor evolution with the fishplot package for R. *BMC Genomics* 2016;**17**:880.

[12] Hu Z, Ding J, Ma Z, Sun R, Seoane JA, Scott Shaffer J, Suarez CJ, Berghoff AS, Cremolini C, Falcone A, et al. Quantitative evidence for early metastatic seeding in colorectal cancer. *Nat Genet* 2019;**51**:1113–22.

[13] Hübschmann D, Jopp-Saile L, Andresen C, Krämer S, Gu Z, Heilig CE, Kreutzfeldt S, Teleanu V, Fröhling S, Eils R, et al. Analysis of mutational signatures with yet another package for signature analysis. *Genes Chromosomes Cancer* 2021;**60**:314–31.

[14] Yates LR, Knappskog S, Wedge D, Farmery JHR, Gonzalez S, Martincorena I, Alexandrov LB, Van Loo P, Haugland HK, Lilleng PK, et al. Genomic evolution of breast cancer metastasis and relapse. *Cancer Cell* 2017;**32** 169-184.e167.

[15] Li T, Fu J, Zeng Z, Cohen D, Li J, Chen Q, Li B, Liu XS. TIMER2.0 for analysis of tumor-infiltrating immune cells. *Nucleic Acids Res* 2020;**48** W509-w514.

[16] Broit N, Johansson PA, Rodgers CB, Walpole ST, Newell F, Hayward NK, Pritchard AL. Meta-analysis and systematic review of the genomics of mucosal melanoma molecular cancer research. *MCR* 2021;**19**:991–1004.

[17] Jurcak NR, Rucki AA, Muth S, Thompson E, Sharma R, Ding D, Zhu Q, Eshleman JR, Anders RA, Jaffee EM, et al. Axon guidance molecules promote perineural invasion and metastasis of orthotopic pancreatic tumors in mice. *Gastroenterology* 2019;**157**:838–50 e836.

[18] Seoane J, Gomis RR. TGF-$\beta$ family signaling in tumor suppression and cancer progression. *Cold Spring Harb Perspect Biol* 2017;**9**.

[19] Heraud C, Pinault M, Lagree V, Moreau V. p190RhoGAPs, the ARHGAP35- and ARHGAP5-encoded proteins, in health and disease. *Cells* 2019;**8**.

[20] van Buul JD, Timmerman I. Small Rho GTPase-mediated actin dynamics at endothelial adherens junctions. *Small GTPases* 2016;**7**:21–31.

[21] Klein CA. Cancer progression and the invisible phase of metastatic colonization. *Nat Rev Cancer* 2020;**20**:681–94.

[22] Risson E, Nobre AR, Maguer-Satta V, Aguirre-Ghiso JA. The current paradigm and challenges ahead for the dormancy of disseminated tumor cells. *Nat Cancer* 2020;**1**:672–80.

[23] Albrengues J, Shields MA, Ng D, Park CG, Ambrico A, Poindexter ME, Upadhyay P, Uyeminami DL, Pommier A, Küttner V, et al. Neutrophil extracellular traps produced during inflammation awaken dormant cancer cells in mice. *Science* 2018;**361**.

[24] Fluegen G, Avivar-Valderas A, Wang Y, Padgen MR, Williams JK, Nobre AR, Calvo V, Cheung JF, Bravo-Cordero JJ, Entenberg D, et al. Phenotypic heterogeneity of disseminated tumour cells is preset by primary tumour hypoxic microenvironments. *Nat Cell Biol* 2017;**19**:120–32.

[25] Bragado P, Estrada Y, Parikh F, Krause S, Capobianco C, Farina HG, Schewe DM, Aguirre-Ghiso JA. TGF-$\beta$2 dictates disseminated tumour cell fate in target organs through TGF-$\beta$-RIII and p38$\alpha$/$\beta$ signalling. *Nat Cell Biol* 2013;**15**:1351–61.

[26] DeVito NC, Plebanek MP, Theivanthiran B, Hanks BA. Role of tumor-mediated dendritic cell tolerization in immune evasion. *Front Immunol* 2019;**10**:2876.

[27] Tucci M, Passarelli A, Mannavola F, Felici C, Stucci LS, Cives M, Silvestris F. Immune system evasion as hallmark of melanoma progression: the role of dendritic cells. *Front Oncol* 2019;**9**:1148.

[28] Peng L, Zhang Y, Wang Z. Immune responses against disseminated tumor cells. *Cancers* 2021;**13**.

[29] Tang M, Diao J, Cattral MS. Molecular mechanisms involved in dendritic cell dysfunction in cancer. *Cell Mol Life Sci: CMLS* 2017;**74**:761–76.